REPORT DOCUMENTATION PAGE

2 6 AFRL-SR-BL-TR-99-

0 115

Public reporting burden for this collection of information is estimated to average 1 hour per response, including the time for reviewing ins
needed, and completing and reviewing this collection of information. Send comments regarding this burden estimate or any other aspe
burden to Washington Headquarters Services, Directorate for Information Operations and Reports, 1215 Jefferson Davis Highway, Sui
Budget, Paperwork Reduction Project (0704-0188), Washington, DC 20503

1. AGENCY USE ONLY (Leave blank)	2. REPORT DATE **April 1999**	3. REPORT TYPE AND DATES COVERED Final Technical Report – 4/1/95 – 9/30/98

4. TITLE AND SUBTITLE Large Eddy Simulation of a Coaxial Jet Combustor	5. FUNDING NUMBERS F49620-95-1-0185

6. AUTHOR(S)

Prof. Parviz Moin
Mr. Charles D. Pierce

7. PERFORMING ORGANIZATION NAME(S) AND ADDRESS(ES) STANFORD UNIVERSITY Mechanical Engineering Flow Physics & Computation Division Bldg. 500, Rm. 500B Stanford, CA 94305-3030	8. PERFORMING ORGANIZATION REPORT NUMBER 2DJA549

9. SPONSORING / MONITORING AGENCY NAME(S) AND ADDRESS(ES) AFOSR/NA Dr. Thomas Beutner 801 N. Randolph Rd., Rm. 732 Arlington, VA 22203-1977	10. SPONSORING / MONITORING AGENCY REPORT NUMBER

11. SUPPLEMENTARY NOTES

12a. DISTRIBUTION / AVAILABILITY STATEMENT APPROVED FOR PUBLIC RELEASE. DISTRIBUTION IS UNLIMITED	12b. DISTRIBUTION CODE

13. ABSTRACT (Maximum 200 Words)

A review of progress in large eddy simulation of complex reacting flows is presented. Topics include: the governing equations for low Mach number combustion, assumed PDF subgrid-scale models, subgrid-scale modeling for the variance and dissipation rate of a conserved scalar, inflow and exit boundary conditions for confined swirling flows, simulation results for isothermal swirling flow with experimental validation, and results from a preliminary reacting flow simulation.

14. SUBJECT TERMS Large Eddy Simulation, Coaxial Jet Combustor, Turbulence, Combustion, Subgrid-Scale Modeling, Reacting Flow Simulation, Swirling Flow		15. NUMBER OF PAGES 17
		16. PRICE CODE

17. SECURITY CLASSIFICATION OF REPORT UNCLASSIFIED	18. SECURITY CLASSIFICATION OF THIS PAGE UNCLASSIFIED	19. SECURITY CLASSIFICATION OF ABSTRACT UNCLASSIFIED	20. LIMITATION OF ABSTRACT

Final Technical Report for the period April 1, 1995 - September 30, 1998 for the grant entitled:

Large Eddy Simulation of a Coaxial Jet Combustor

Parviz Moin and Charles C. Pierce

Stanford University

Mechanical Engineering, Flow Physics & Computation Division

Stanford, CA 94305-3030

19990503 061

LARGE EDDY SIMULATION OF A COAXIAL JET COMBUSTOR

AFOSR F49620-95-1-0185 Final Report

Parviz Moin and Charles D. Pierce

Department of Mechanical Engineering
Stanford University, Stanford, CA 94305-3030

Abstract

A review of progress in large eddy simulation of complex reacting flows is presented. Topics include: the governing equations for low Mach number combustion, assumed PDF subgrid-scale models, subgrid-scale modeling for the variance and dissipation rate of a conserved scalar, inflow and exit boundary conditions for confined swirling flows, simulation results for isothermal swirling flow with experimental validation, and results from a preliminary reacting flow simulation.

1. Introduction

The coaxial jet combustor is an idealized gas turbine combustor geometry for which a number of experiments have been performed under a variety of conditions, both reacting and non-reacting. Figure 1 shows a schematic of a coaxial jet combustor in which gaseous fuel is supplied to the central pipe, and swirling air is supplied to the surrounding annulus. The two streams begin mixing after a sudden expansion and then react in a swirl-stabilized diffusion flame.

Because of the availability of experiments, this configuration was chosen as the context for the development of large eddy simulation (LES) based prediction methods for complex reacting flows. It is expected that LES will become an important tool for analysis of flows that are not easily modeled using Reynolds average approaches or in which unsteady dynamics of the large scales are important to understanding or predicting flow behavior. Turbulent reacting flows appear to satisfy both of these conditions and thus represent a promising and technologically important application for LES.
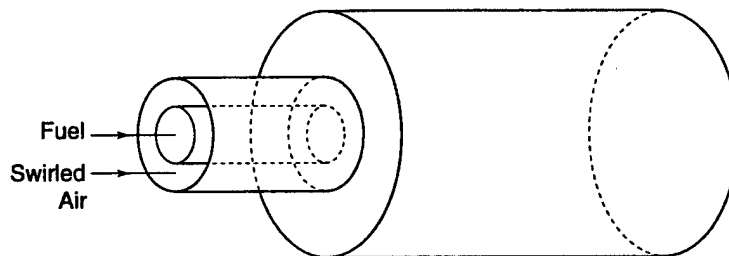

Fig. 1 Schematic of a coaxial jet combustor.

Johnson and Bennett[1] conducted experiments of non-reacting confined coaxial jets using water with Reynolds number 80,300 based on overall mass flow rate and jet diameter. Roback and Johnson,[2] using the identical configuration, later extended the measurements

1

to include swirl in the annular stream with a swirl number of approximately 0.41. Sommerfeld et al.[3] performed experiments in a slightly different configuration with particle-laden air (Reynolds number 52,400 and swirl number 0.47, based on overall jet properties). Owen et al.[4] performed a series of reacting experiments with methane and air under a range of flow conditions.

Akselvoll and Moin[5,6] completed a large eddy simulation study of the non-swirling, non-reacting coaxial jet. They included a passive scalar in their calculations to investigate mixing between the central and annular jets and validated their results against the experiment of Johnson and Bennett.[1] The present study focuses on the effects of swirl and heat release and on subgrid models for turbulent combustion.

The topics and issues discussed in this paper include: the governing equations for low Mach number combustion (Sec. 2), subgrid-scale modeling for these equations including proposed dynamic models for subgrid-scale variance and dissipation rate of a conserved scalar (Sec. 3), the numerical techniques used in this study including a novel method for generating swirling inflow boundary conditions (Sec. 4), results for isothermal swirling flow including the effect of exit boundary conditions on confined swirling flows (Sec. 5), and the effects of heat release as found in a preliminary reacting simulation (Sec. 6).

2. Governing Equations

We consider the variable density momentum and conserved scalar transport equations:

$$\frac{\partial \rho \mathbf{u}}{\partial t} + \nabla \cdot (\rho \mathbf{u} \mathbf{u}) = -\nabla p + \nabla \cdot \left[2\mu (\mathbf{S} - \tfrac{1}{3}\mathbf{I} \nabla \cdot \mathbf{u}) \right] \tag{1}$$

$$\frac{\partial \rho \phi}{\partial t} + \nabla \cdot (\rho \mathbf{u} \phi) = \nabla \cdot (\rho \alpha \nabla \phi) \tag{2}$$

where, $\mathbf{S}$ is the strain-rate tensor, $\mathbf{I}$ is the identity tensor, ϕ is any transported scalar, and α is the molecular diffusivity of the scalar. The *low Mach number* approximation is invoked so that only the uniform background pressure p_0 enters into the ideal gas equation of state:

$$\rho = \frac{p_0}{RT} \tag{3}$$

This effectively decouples the density from the pressure and precludes the formation and propagation of acoustic waves. The low Mach number approximation also allows the energy equation to be written in conserved scalar form (2). Since the density is determined by the equation of state, the continuity equation becomes a constraint on the velocity field, with the time-derivative of density as a source term:

$$\nabla \cdot (\rho \mathbf{u}) = -\frac{\partial \rho}{\partial t} \tag{4}$$

This constraint is enforced by the pressure, in a manner analogous to the enforcement of the incompressibility constraint for isothermal flows.

With the additional assumptions of *fast chemistry* and *unity Lewis number*, the density, as well as temperature and all chemical species, can be directly related to the conserved

2

scalar mixture fraction Z, which satisfies (2). The equation of state then reduces to a density function, $\rho = \rho(Z)$. Figure 2 illustrates a specific form of the dependence. The flame is located at the stoichiometric value of the mixture fraction, Z_{st}, where temperature is a maximum and density is a minimum (cf. Ref. 7).

When the fast chemistry and unity Lewis number assumptions are relaxed and more general combustion models such as laminar flamelets[8] are used, the density function can be extended to include more independent variables such as the scalar dissipation rate χ. This more general equation of state is written as:
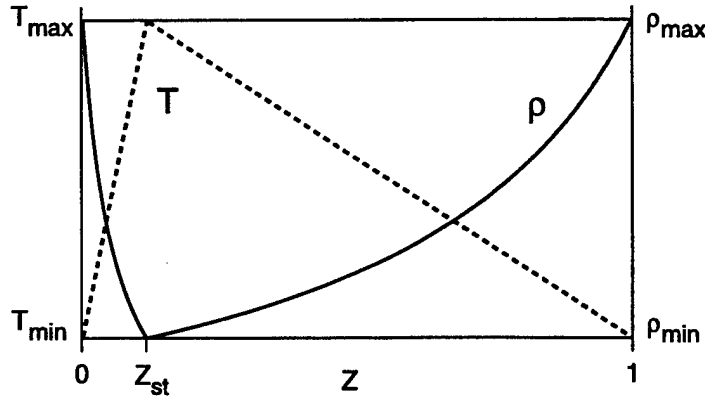
$$\rho = \rho(Z, \chi, \ldots) \tag{5}$$

Fig. 2 Typical dependence of density and temperature on mixture fraction from the fast chemistry assumption.

The determination of the continuity constraint source term $-\frac{\partial \rho}{\partial t}$ presents some difficulty. It can be determined in principle by differentiating the equation of state with respect to time. But this is impractical because the functional dependence (5) can be arbitrarily complex and may include contributions from subgrid-scale models (discussed in Sec. 3) and chemical reaction models. The typical approach is to approximate the time-derivative of density by finite difference in time.

3. Subgrid-Scale Modeling

The LES formalism[9] introduces a filtering operation that is applied to the governing equations and flow variables to remove the unresolved small scales. As a result of filtering the nonlinear terms, unclosed subgrid-scale terms analogous to the unclosed terms in Reynolds averaged approaches appear in the equations. Grid-filtering is indicated using an overbar, and a tilde is used to indicate density weighted (Favre) grid-filtering, $\tilde{\phi} = \overline{\rho\phi}/\bar{\rho}$, so that $\tilde{\phi}$ is the resolved scalar field computed directly by LES.

Subgrid momentum and scalar transport terms that appear in equations (1) and (2) are modeled using the dynamic approach of Moin et al.[10] The other major modeling requirement is for the nonlinear density function (5). One needs to obtain the filtered density,

$$\bar{\rho} = \overline{\rho(Z, \chi, \ldots)} \tag{6}$$

3

but the scalar transport equation provides only the filtered mixture fraction $\widetilde{Z}$, and

$$\overline{\rho(Z, \chi, \ldots)} \neq \rho(\widetilde{Z}, \overline{\chi}, \ldots)$$

because of the nonlinearity.

A general method of evaluating a nonlinear expression such as (6) is to express it in terms of the probability density function (PDF) of the independent variables. In the present discussion we restrict our attention to the case of fast chemistry, which implies that ρ is only a function of Z. If the PDF of the subgrid mixture fraction fluctuation $P(Z)$ were known, the filtered density could be evaluated using

$$\overline{\rho} = \overline{\rho(Z)} = \int \rho(Z) P(Z)\, dZ \qquad (7)$$

The PDF can be modeled directly by assuming a particular analytical form for it. Frankel et al.[11] and Cook and Riley[12] proposed using the Beta family of distributions, parameterized by the mean and variance. Two examples of Beta distributions are plotted in Fig. 3. When the subgrid-scale is mostly mixed and the variance is small, the PDF is similar to a Gaussian distribution. But when the variance is large, the distribution becomes bimodal, representing a subgrid-scale state that is mostly unmixed. Although its usefulness in Reynolds average modeling has been questioned, the assumed Beta PDF was recently shown to accurately represent the subgrid-scale mixture fraction in LES by Jiménez et al.[13], who performed a priori tests in a turbulent mixing layer.
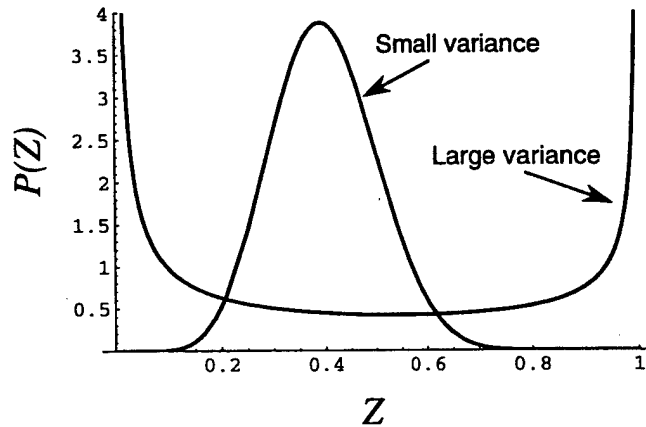

Fig. 3 Typical Beta distributions.

Once particular values of the mean and variance are specified, the corresponding Beta PDF is known and can be substituted into (7) and integrated to obtain the filtered density. In this way, the density can be precomputed and stored into a lookup table, to be retrieved during the simulation as a function of the resolved mixture fraction field $\widetilde{Z}$ (the mean), and the subgrid-scale mixture fraction variance $\widetilde{Z''^2}$,
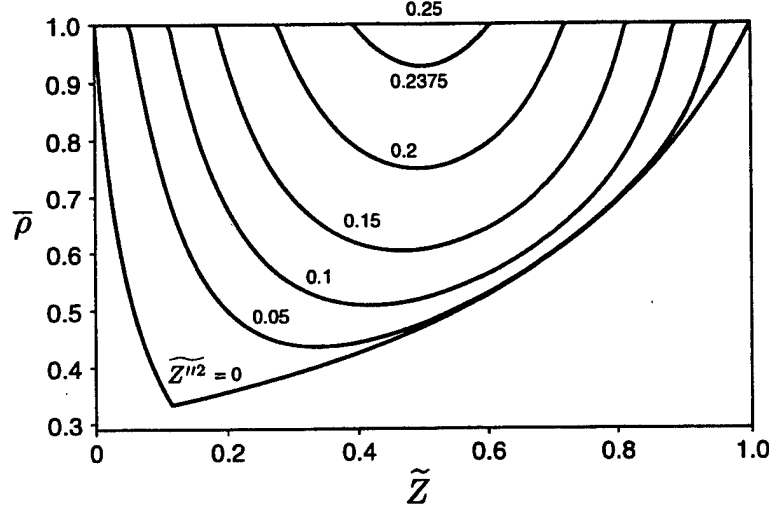
$$\overline{\rho} = f(\widetilde{Z}, \widetilde{Z''^2})$$

4

Fig. 4 A lookup table for density as a function of $\widetilde{Z}$ and $\widetilde{Z''^2}$ for fast chemistry and the Beta PDF.

An example of a lookup table is shown in Fig. 4. The curve for zero variance is the same as the original density function $\rho(Z)$ in Fig. 2. As the variance is increased, the subgrid field becomes increasingly unmixed and therefore unburned, leading to higher densities. The mean $\widetilde{Z}$ is known from the scalar transport equation (2), but the variance requires additional modeling. A model for the subgrid variance of a conserved scalar is discussed next.

Subgrid-Scale Variance

To predict the subgrid-scale variance of a conserved scalar, Cook and Riley[12] proposed a scale similarity model, which they showed through a-priori tests in homogeneous isotropic turbulence, yielded accurate predictions. The model has since been used in an LES of nonpremixed combustion in homogeneous isotropic turbulence[14] and a priori tested in a turbulent mixing layer.[13] The major drawback of this approach is that it requires input from the user in the form of a model coefficient. Furthermore, there is no reason to expect that a 'universal' value for the model coefficient exists, except within a well developed inertial subrange. In general, the coefficient could vary with flow type, characteristics of the grid and test filters, Reynolds and Péclet numbers, etc. Recently, some attempt has been made to determine the dependence of the coefficient on such parameters.[15] This limitation can be overcome, in principle, by using the Dynamic Procedure[10,16−18] combined with an appropriate scaling law, in which model coefficients are determined automatically in response to local flow conditions.

For the purpose of modeling subgrid Favre variance $\widetilde{\phi''^2}$ of a conserved scalar ϕ the following scaling law has been proposed[19]:

$$\overline{\rho}\,\widetilde{\phi''^2} = C\Delta^2\,\overline{\rho}\,|\nabla\widetilde{\phi}|^2 \tag{8}$$

The local filter width, Δ, serves as the length scale of the subgrid turbulence. Eq. (8) is analogous to Yoshizawa's expression[20] for the subgrid kinetic energy and can be found
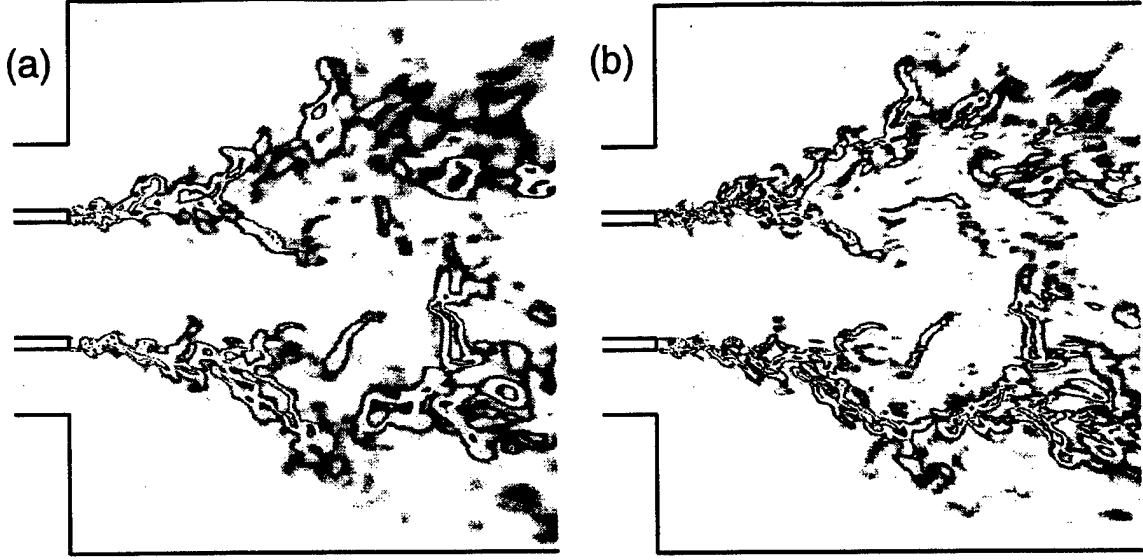
5

Fig. 5 Comparison of predicted subgrid-scale variance in a meridional plane using the (a) scale-similarity model, and (b) dynamic model.

through consideration of the transport equation for the subgrid-scale variance, combined with the local equilibrium assumption.

We now apply the Dynamic Procedure to obtain the model coefficient C in (8). To simplify notation, we introduce the density-weighted test-filtered scalar field, $\breve{\phi}$, defined by:

$$\breve{\phi} = \frac{\widehat{\overline{\rho}\widetilde{\phi}}}{\widehat{\overline{\rho}}} \tag{9}$$

A hat indicates test filtering at a scale larger than the grid filter, $\widehat{\Delta}$, usually taken to be twice the grid filter width. We also define the Leonard term,

$$\mathcal{L} = \widehat{\overline{\rho}\widetilde{\phi}^2} - \widehat{\overline{\rho}}\,\breve{\phi}^2 \tag{10}$$

and the model term,

$$\mathcal{M} = \widehat{\Delta}^2\,\widehat{\overline{\rho}}\,|\nabla\breve{\phi}|^2 - \Delta^2\,\widehat{\overline{\rho}|\nabla\widetilde{\phi}|^2} \tag{11}$$

Note that the scale similarity model[12] can be expressed using this notation as

$$\overline{\rho}\,\widetilde{\phi''^2} = C_s\,\mathcal{L} \tag{12}$$

where C_s is the unknown scale-similarity coefficient. Next, using the identity,

$$\left(\widehat{\overline{\rho}\widetilde{\phi}^2} - \widehat{\overline{\rho}}\,\breve{\phi}^2\right) - \widehat{\left(\overline{\rho}\widetilde{\phi}^2 - \overline{\rho}\widetilde{\phi}^2\right)} = \mathcal{L} \tag{13}$$

6

and assuming that, while the model coefficient may vary in space and time, the same coefficient applies to both filter levels, one obtains $\mathcal{L} = C\mathcal{M}$. Although C could be determined locally using $C = \mathcal{L}/\mathcal{M}$, least-squares averaging should be performed over the statistically homogeneous directions to obtain a more accurate (and stable) value. For fully inhomogeneous flows, the more general Dynamic Localization Procedure of Ghosal et al.[18] should be used. With statistical averaging over homogeneous directions indicated by angle brackets, the final expression for the model coefficient is

$$C = \frac{\langle \mathcal{L}\mathcal{M} \rangle}{\langle \mathcal{M}^2 \rangle} \tag{14}$$

The dynamic and scale-similarity models have been tested in the large eddy simulation (presented in Sec. 6) of the Roback and Johnson[2] configuration with heat release. In Fig. 5, the performance of the dynamic model is compared qualitatively to the predictions of the scale similarity model of Cook and Riley.[12] A value of $C_s \simeq 0.5$ yielded values of roughly the same magnitude as the dynamic model and was used to obtain Fig. 5a. The two model predictions are similar, but the dynamic model is seen to provide a sharper subgrid variance field with more fine scale structure due to its direct dependence on the resolved scalar gradient $|\nabla \widetilde{\phi}|$. The scale-similarity model generally predicted significantly higher levels of variance, though the overall level depends on the value chosen for C_s.

Scalar Dissipation Rate

The dissipation rate of the variance of a conserved scalar is needed as a parameter in flamelet models of nonpremixed combustion.[21] Even though an appropriate scaling law for the subgrid-scale dissipation rate can be derived, the Dynamic Procedure cannot be applied directly to this problem because virtually all of the dissipation occurs at the smallest unresolved scales. Instead, the approach adopted here is to determine the subgrid variance *production* rate and assume that the subgrid dissipation and production rates are in equilibrium. A similar model was previously proposed by Girimaji and Zhou,[22] though they obtained it starting from different assumptions and using spectral transfer arguments.

The assumption that the subgrid scales are in local equilibrium with the large scales leads to a simple model for the subgrid scalar dissipation rate χ_{SGS}. In equilibrium, χ_{SGS} is equal to the local subgrid variance production rate, $-\overline{\rho}\,\widetilde{(u_j''\phi'')}\,\widetilde{\phi}_{,j}$ (repeated indices imply summation and a subscripted comma indicates partial differentiation), which can be obtained by assuming a gradient diffusion model for the turbulent scalar flux and using the dynamic model of Moin et al.[10] for the turbulent scalar-diffusivity $\alpha_t = C_\alpha \Delta^2 |\widetilde{S}|$. One then obtains $\chi_{\text{SGS}} = \overline{\rho}\,\alpha_t\,|\nabla \widetilde{\phi}|^2$. If the resolved dissipation rate is included, the total filtered dissipation rate becomes

$$\overline{\chi} = \overline{\rho}(\alpha + \alpha_t)\,|\nabla \widetilde{\phi}|^2 \tag{15}$$

where α is the molecular scalar-diffusivity. Note that with this model, $\overline{\chi}$ can be obtained at virtually no additional computational cost, since α_t would have already been computed for modeling the turbulent scalar flux in the transport equation for the resolved scalar field.
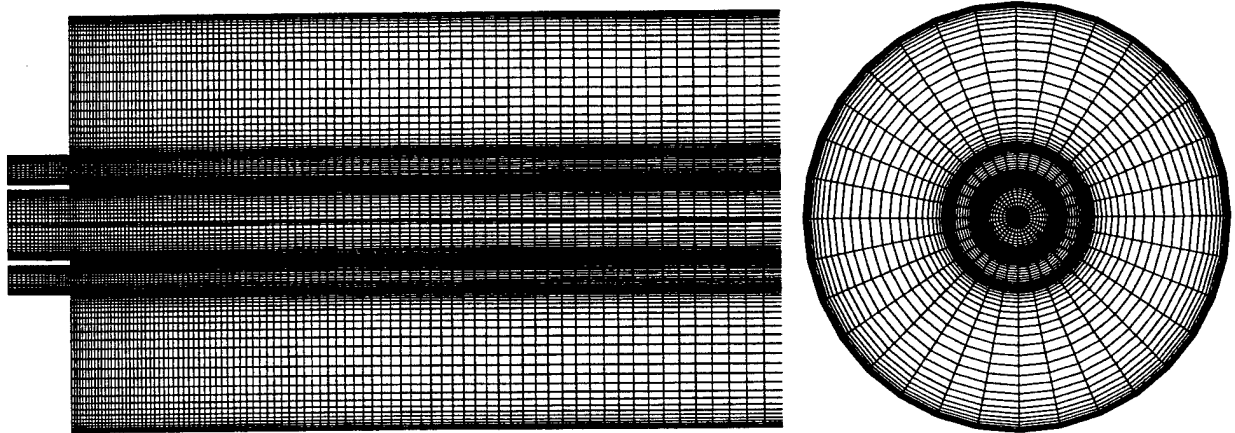
Fig. 6 Typical grid discretization in cylindrical coordinates.

4. Numerics

The governing transport equations (1) and (2) are solved in cylindrical coordinates. Fig. 6 shows a typical discretization, which includes grid refinement near solid surfaces. The numerical scheme consists of conservative, second-order finite-volumes on staggered grids. A second order, semi-implicit time advancement approach, in which the derivatives along a single coordinate direction are treated implicitly, is used to remove the CFL restriction of near-wall grid refinement and the convergence of the radial coordinate lines near the centerline. Details are provided by Akselvoll and Moin.[5] The equation of state (3) is conveniently and efficiently evaluated from the independent variables (Z, χ, etc.) by precomputing the density function and storing it into a lookup table. The continuity constraint (4) is enforced at each time step by solving a Poisson equation for the pressure. Fast Fourier transforms are applied in the azimuthal direction to factor the three-dimensional Poisson equation into a set of two-dimensional Helmholtz equations. The Helmholtz equations are then solved with either a line-relaxation scheme or multigrid scheme.

Swirl Generation

Physically, swirl is generated by tangential jets or contoured or plane vanes, which are difficult to simulate numerically. As modern simulation and experimental methods allow for more detailed characterization of flow behavior, it has become increasingly important to provide well-defined, reproducible inlet conditions. This problem has not been previously addressed for swirling flows.

Computation of turbulent swirling flows has been carried out mostly in the Reynolds averaged turbulent flow prediction context. There, the inflow condition is usually determined by specifying either experimental data or else simple algebraic mean profiles. Further discussion is provided in a review article by Sloan, Smith, and Smoot.[23] The present study appears to be the first attempt at large eddy simulation of turbulent swirling flows. The azimuthal body force technique described here represents a means of predicting, rather than prescribing, swirling inflow boundary conditions.
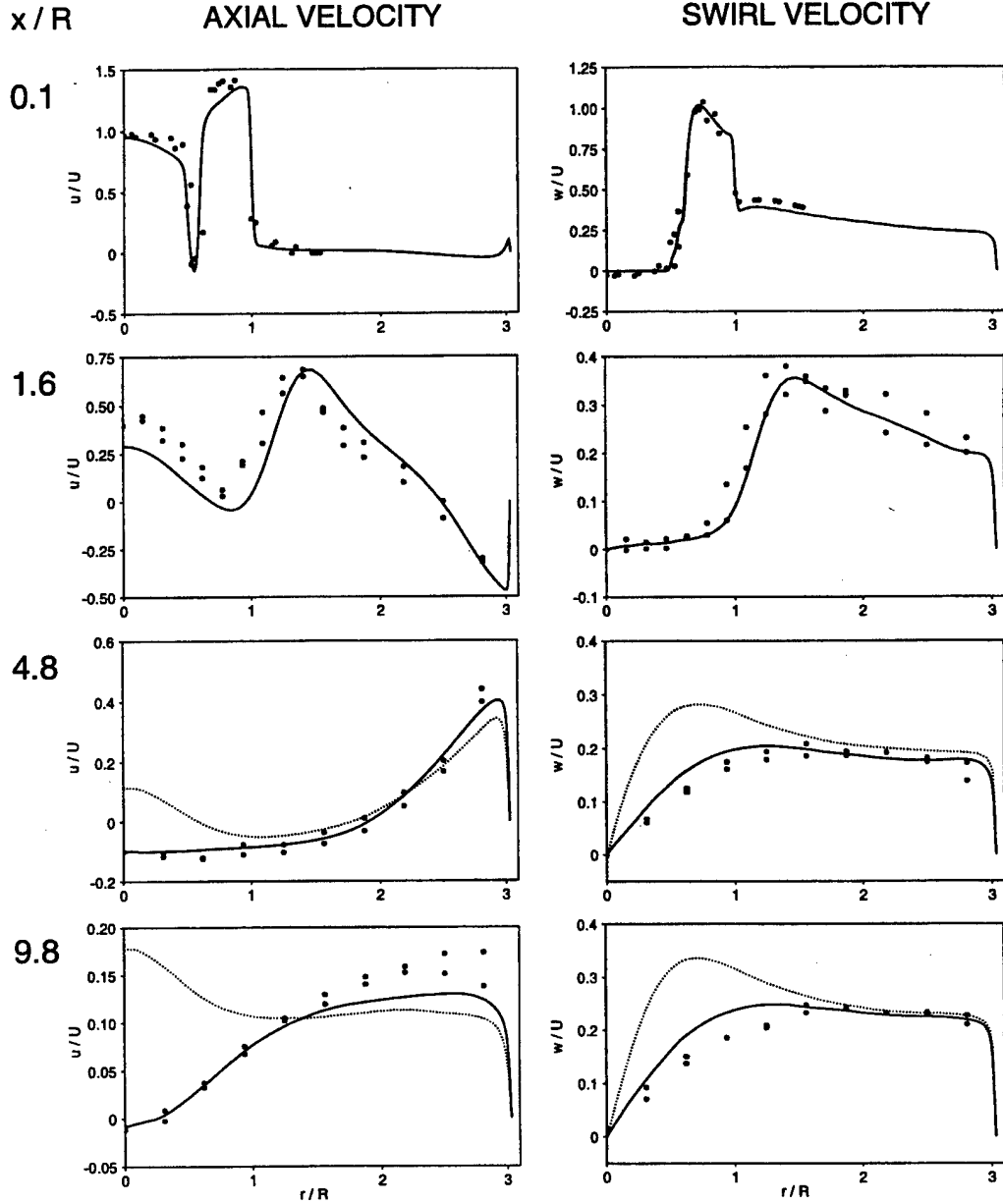
8

x / R   AXIAL VELOCITY   SWIRL VELOCITY

Fig. 7 Comparison of predicted radial profiles of axial and azimuthal velocity with experimental data of Sommerfeld et al.[3]: ———— LES $226 \times 163 \times 128$ grid, corresponding to the bottom of Fig. 9; ······ LES corresponding to the top of Fig. 9; ● experiment.

Equilibrium swirling flows can be generated numerically by solving for the flow driven by fictitious axial and azimuthal body forces in a spatially periodic pipe, from which data is fed as inflow boundary condition into the main computational domain. The axial body force represents the mean pressure gradient which drives the physical flow and has long been established as a means of driving spatially periodic pipe and channel flows. On the other hand the azimuthal body force, used to drive the swirl component, is not physically producible and should be thought of as existing only to overcome drag from the walls. The
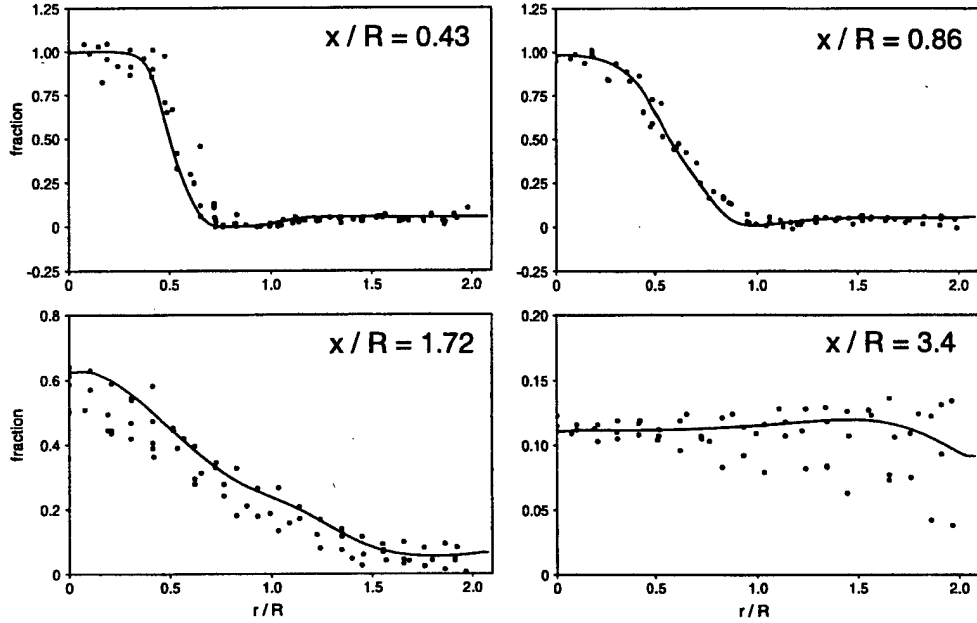
9

Fig. 8 Comparison of predicted radial profiles of mixture fraction (passive scalar) with experimental data of Roback and Johnson[2]: —— LES 250 × 125 × 64 grid; • experiment.

resulting flow is a stationary approximation to slowly decaying swirl.

The radial profile of the axial body force $f_x(r)$ is taken to be uniform as in the Poiseuille flow. For the swirling case there does not exist a corresponding physical mechanism for driving the flow, so there is some freedom in choosing the forcing profile $f_\theta(r)$. Tests revealed that the flow is rather insensitive to the forcing distribution used. A uniform body force appeared to be adequate, and for simplicity, it was chosen for use in all subsequent simulations. Details and further discussion will appear in a forthcoming article.[24]

5. Isothermal Flow with Swirl

The equations governing isothermal flow are Eqs. (1), (2), and (4) with $\rho = $ const. We consider the incompressible flow experiments of Roback and Johnson[2] and Sommerfeld et al.[3] Figures 7 and 8 present a comparison of the computed mean velocity and mixture fraction profiles with experimental data. Although a few discrepancies can be seen, overall agreement is good. In particular, note the agreement at the axial station closest to the inlet which shows the effectiveness of the above swirl generation method.

While the Reynolds average approach has been fairly successful at predicting the velocity field for swirling flows, it has been much less successful at predicting scalar mixing.[25] The LES approach, on the other hand, can give very accurate predictions as evidenced in Fig. 8, probably due to its accurate representation of the large scale mixing.

Exit Boundary Conditions

The simulations have shown that exit boundary conditions can have a tremendous influence on confined swirling flows. The presence of a contraction or expansion at the end of

10

the test section can completely change the character of the upstream central recirculation zone. This has been observed in experiments[26] and has been known in vortex breakdown computations, but was not previously reported in turbulence simulations. Early simulations using the convective outflow boundary condition[27] produced the flow depicted at the top of Fig. 9, contrary to the experimental results.[3] In later simulations, the geometry was modified by adding a second expansion at the outflow boundary to represent the effect of a stagnation chamber at the end of the experimental test section.[3] This modification produced a very different flowfield, shown in the bottom of Fig 9, that compares well with the experiment.[3]

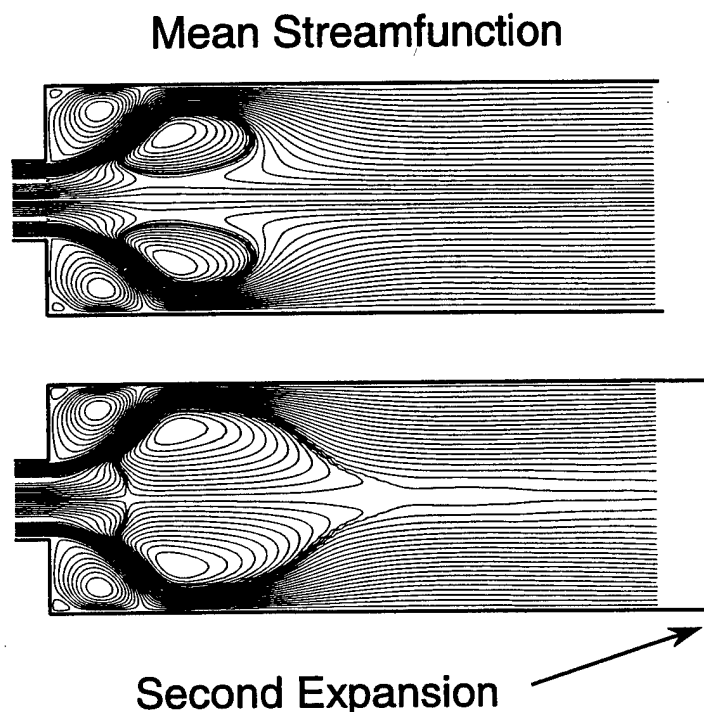## Mean Streamfunction

Second Expansion

Fig. 9 Effect of downstream boundary conditions on a confined swirling flow. The character of the central recirculation zone is completely changed by the addition of a second expansion to the geometry.

Perhaps the best way to understand this phenomenon is to consider the behavior of the pressure in a swirling flow. Whenever there is swirl or rotation in a flow, a radial pressure gradient must exist to balance the centrifugal force. Without an exit expansion a strong vortex core naturally develops, thereby decreasing the pressure along the centerline and creating a favorable axial pressure gradient which may further enhance the development of the vortex core. The effect of the exit expansion is to force the pressure to become radially uniform at the exit plane, causing an adverse axial pressure gradient along the centerline that may influence the development of the flow all the way back to the inlet.

Escudier and Keller[26] studied the effect of exit contraction on confined swirling flows but did not consider whether exit expansion would have any effect. They also speculated that reacting flows would not be susceptible to the exit boundary condition because of

11

substantially reduced density and increased axial velocity due to heat release. Apparently, Reynolds average calculations of confined swirling flows have not shown such sensitivity to exit boundary conditions.

6. Reacting Flow with Swirl and Heat Release

As a first step towards simulation and modeling of real reacting systems, the capability of the variable density formulation to capture effects of heat release was tested in an idealized combustion system, by assuming infinitely fast reaction of the fuel and oxidizer streams in the Roback and Johnson[2] configuration. The present results are preliminary in that they have not been validated against experimental data.
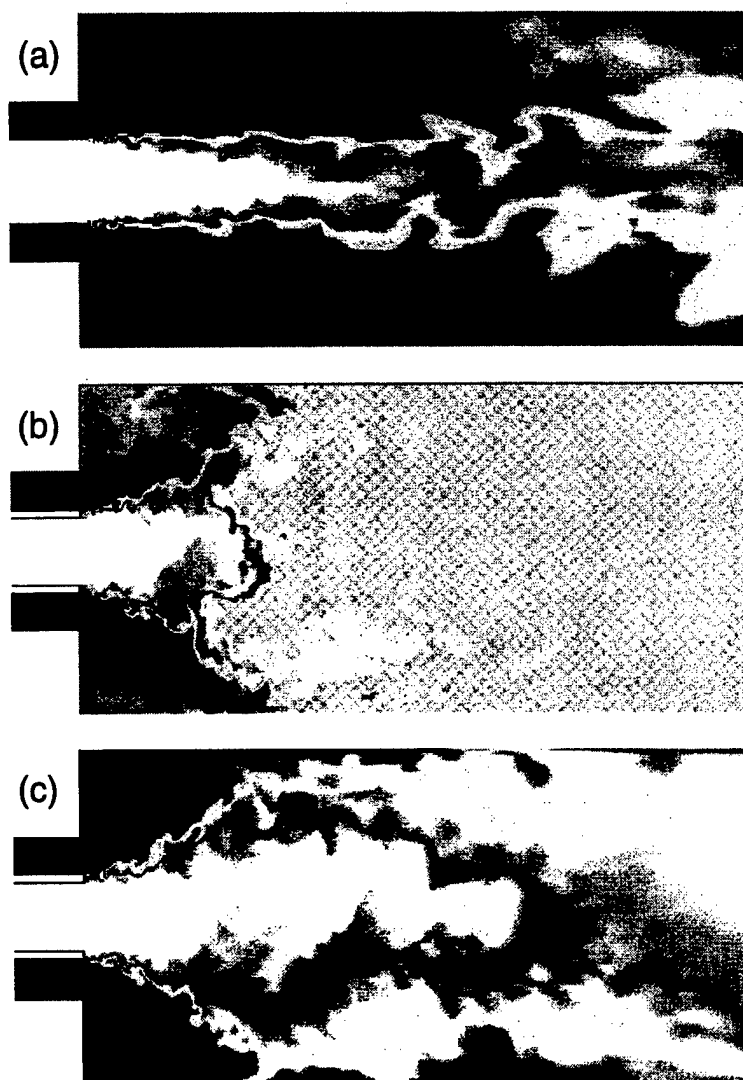

Fig. 10 Comparison of mixture fraction fields for (a) non-swirling isothermal flow, (b) swirling isothermal flow, and (c) swirling flow with heat release in identical configurations. Black: air, white: fuel, and gray: mixed.

The combustion parameters for this case were chosen to reflect typical conditions in a practical combustor. The density ratio, ρ_{max}/ρ_{min}, was taken to be 3, which is consistent with preheated air from the compressor, and the equivalence ratio was set to 0.9. Fig. 10 compares snapshots of the mixture fraction for this case and two previous isothermal cases, all from the same Johnson-Bennett-Roback[1,2] configuration. In the non-swirling isothermal case, the fuel and oxidizer streams mix very gradually. When swirl is added, the mixing effectiveness of the flow increases dramatically. When heat release is added, the mixing region is pushed outward as the flow accelerates, and the mixing efficiency is substantially reduced. The annular air flows around the central mixing zone and impinges on the outer wall, forming a wall jet which acts to confine the core flow.

Fig. 11 shows a quantitative comparison of the mean velocity profiles for the isothermal and reacting cases. Near the expansion point, before much heat release has occurred, the profiles are very similar, but further downstream, one can see the axial flow being accelerated by the heat release. On the other hand, the swirl component of velocity is largely unaffected by the heat release, as can be expected from the fact that the density variations are axisymmetric on average.

7. Conclusion

Large eddy simulation of a coaxial jet combustor with swirl was performed. The velocity and concentration profiles are in good agreement with experiments. It was shown that confined swirling flows can be very sensitvie to downstream boundary conditions. To account for the effects of heat release a low Mach number variable density formulation for LES was developed and implemented. An assumed PDF approach was used to model the subgrid-scale mixture fraction in the limit of fast chemistry, and a new dynamic model was used to compute the variance of the subgrid mixture fraction as input to the assumed PDF. Simulation results showed that heat release reduces mixing and, as expected, accelerates the flow in the combustor.

8. Future Directions

Subgrid models to account for finite-rate chemistry need to be developed and validated against combustion experiments such as Owen et al.[4] The benchmark experiments of a piloted methane/air jet (Barlow et al., Combustion Research Facility, Sandia National Laboratory) will be simulated to provide detailed validation of the chemistry model. An extension of the low Mach number equations to incorporate low frequency acoustics will be used to capture acoustic combustion instabilities. The resulting simulation capabilities will be used to develop active control strategies to suppress instability and improve combustor performance. It is hoped that this effort will continue under support from the AFOSR propulsion program.
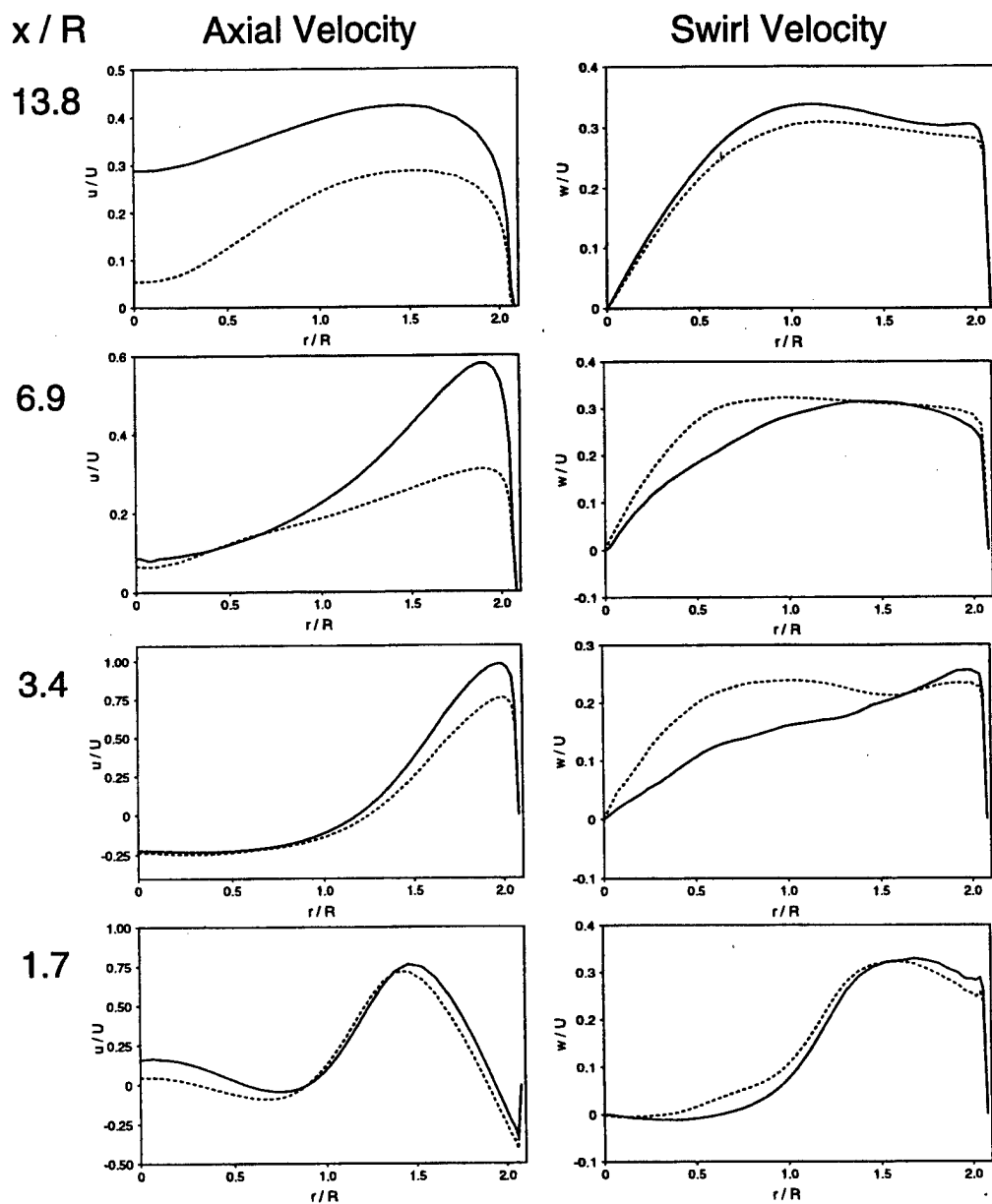
Fig. 11 Radial profiles of axial and azimuthal velocity components showing the effect of heat release: − − − isothermal, ——— with heat release.

References

1. Johnson, B. V. and Bennett J. C. "Statistical Characteristics of Velocity, Concentration, Mass Transport, and Momentum Transport for Coaxial Jet Mixing in a Confined Duct" *J. Eng. Gas Turbines and Power* **106**, 121–127 (1984)

2. Roback, R. and Johnson, B. V. "Mass and momentum turbulent transport experiments with confined swirling coaxial jets" NASA CR-168252 (1983)

3. Sommerfeld, M., Ando, A. and Wennerberg, D. "Swirling, particle-laden flows through a pipe expansion" *J. Fluids Eng.* **114**, 648–656 (1992)

4. Owen, F. K., Spadaccini, L. J. and Bowman, C. T. "Pollutant formation and energy release in confined turbulent diffusion flames" Sixteenth Symposium (international) on Combustion p. 105, The Combustion Institute (1976)

5. Akselvoll, K. & Moin, P. "An Efficient Method for Temporal Integration of the Navier-Stokes Equations in Confined Axisymmetric Geometries" *J. Comp. Phys.* **125**, 454–463 (1996)

6. Akselvoll, K. & Moin, P. "Large-eddy simulation of turbulent confined coannular jets" *J. Fluid Mech.* **315**, 387–411 (1996)

7. Bilger, R. W. "Turbulent Flows with Nonpremixed Reactants" in *Turbulent Reacting Flows*, P. A. Libby and F. A. Williams, Eds., Springer-Verlag, pp. 65–113 (1980)

8. Peters, N. "Laminar Diffusion Flamelet Models in Non-Premixed Turbulent Combustion" *Prog. Energy Combust. Sci.* **10**, 319–339 (1984)

9. Ghosal, S. and Moin, P. "The Basic Equations for the Large Eddy Simulation of Turbulent Flows in Complex Geometry" *J. Comp. Phys.* **118**, 24–37 (1995)

10. Moin, P., Squires, K., Cabot, W. and Lee, S. "A dynamic subgrid-scale model for compressible turbulence and scalar transport" *Phys. Fluids A* **3**, 2746–2757 (1991)

11. Frankel, S. H., Adumitroaie, V., Madnia, C. K. and Givi, P. "Large eddy simulation of turbulent reacting flows by assumed PDF methods" in *Engineering Applications of Large Eddy Simulations*, 81–101, ASME (1993)

12. Cook, A. W. and Riley, J. J. "A subgrid model for equilibrium chemistry in turbulent flows" *Phys. Fluids* **6**, 2868–2870 (1994)

13. Jiménez, J., Liñán, A., Rogers, M. M. and Higuera, F. J. "A-priori testing of sub-grid models for chemically reacting nonpremixed turbulent shear flows" *Proceedings of the 1996 Summer Program*, Center for Turbulence Research, NASA-Ames / Stanford Univ., 89–110 (1996)

14. Réveillon, J. and Vervisch, L. "Response of the dynamic LES model to heat release induced effects" *Phys. Fluids* **8**, 2248–2250 (1996)

15. Cook, A. W. "Determination of the constant coefficient in scale similarity models of turbulence" *Phys. Fluids* **9**, 1485–1487 (1997)

16. Germano, M., Piomelli, U., Moin, P. and Cabot, W. H. "A dynamic subgrid-scale eddy viscosity model" *Phys. Fluids A* **3**, 1760–1765 (1991)

17. Lilly, D. K. "A proposed modification of the Germano subgrid-scale closure method" *Phys. Fluids A* **4**, 633–635 (1992)

18. Ghosal, S., Lund, T. S., Moin, P. and Akselvoll, K. "A dynamic localization model for large-eddy simulation of turbulent flows" *J. Fluid Mech.* **286**, 229–255 (1995)

19. Pierce, C. D. and Moin, P. "A dynamic model for subgrid-scale variance and dissipation rate of a conserved scalar" to be submitted to *Phys. Fluids* (1998)

20. Yoshizawa, A. "Statistical theory for compressible turbulent shear flows, with the application to subgrid modeling" *Phys. Fluids* **29**, 2152 (1986)

21. Cook, A. W., Riley, J. J. and Kosály, G. "A Laminar Flamelet Approach to Subgrid-Scale Chemistry in Turbulent Flows" *Combust. Flame* **109**, 332–341 (1997)

22. Girimaji, S. S. and Zhou, Y. "Analysis and modeling of subgrid scalar mixing using numerical data" *Phys. Fluids* **8**, 1224–1236 (1996)

23. Sloan, D. G., Smith, P. J., and Smoot, L. D. "Modeling of swirl in turbulent flow systems" *Prog. Energy Combust. Sci.* **12**, 163–250 (1986)

24. Pierce, C. D. and Moin, P. "A Method for Generating Equilibrium Swirling Inflow Conditions" to appear in *AIAA J.* (1998)

25. Brankovic, A., Pratt & Whitney, West Palm Beach, FL. Private communication (1998)

26. Escudier, M. P. and Keller, J. J. "Recirculation in swirling flow: A manifestation of vortex breakdown" *AIAA J.* **23**, 111–116 (1985)

27. Pauley, L. L., Moin, P. and Reynolds, W. C. "The structure of two-dimensional separation" *J. Fluid Mech.* **220**, 397–411 (1990)